19. J. Kalb, F. Spaepen, M. Wuttig, *J. Appl. Phys.* **93**, 2389 (2003).
20. J. Kalb, F. Spaepen, M. Wuttig, *Appl. Phys. Lett.* **84**, 5240 (2004).
21. S. Ziegler, M. Wuttig, *J. Appl. Phys.* **99**, 064907 (2006).
22. S. Senkader, C. D. Wright, *J. Appl. Phys.* **95**, 504 (2004).
23. J. H. Coombs, A. P. J. M. Jongenelis, W. van Es-Spiekman, B. A. J. Jacobs, *J. Appl. Phys.* **78**, 4906 (1995).
24. S. Raoux *et al.*, *IBM J. Res. Dev.* **52**, 465 (2008).
25. T. Matsunaga, Y. Umetani, N. Yamada, *Phys. Rev. B* **64**, 184116 (2001).
26. R. Bez, R. J. Gleixner, F. Pellizzer, A. Pirovano, G. Atwood, in *Phase Change Materials: Science and Applications*, S. Raoux, M. Wuttig, Eds. (Springer, New York, 2009), pp. 355–380.
27. A. N. Pargellis, *J. Vac. Sci. Technol. A* **7**, 27 (1989).
28. V. Weidenhof, I. Friedrich, S. Ziegler, M. Wuttig, *J. Appl. Phys.* **89**, 3168 (2001).
29. M.-H. Kwon *et al.*, *Appl. Phys. Lett.* **90**, 021923 (2007).
30. We thank Y. Xiao, M. Jurich, Y.-C. Chen, M. Salinga, and M. Hitzbleck for their help with thin-film growth and thermal treatments. This material is based on work conducted under IBM-UIUC joint study agreement and is supported by NSF under awards DMR 04-12939 and DMR 07-06267. The FTEM technique was available thanks to collaborative support under award DMR 06-05890. FTEM, AFM, and thermal treatments were carried out, in part, in the Frederick Seitz Materials Research Laboratory Central Facilities, University of Illinois, which are partially supported by the U.S. Department of Energy under grants DE-FG02-07ER46453 and DE-FG02-07ER46471.

Supporting Online Material
www.sciencemag.org/cgi/content/full/326/5955/980/DC1
Materials and Methods
Figs. S1 to S5
References

9 June 2009; accepted 11 September 2009
10.1126/science.1177483

Partitioning Recent Greenland Mass Loss

Michiel van den Broeke,[1]* Jonathan Bamber,[2] Janneke Ettema,[1] Eric Rignot,[3,4] Ernst Schrama,[5] Willem Jan van de Berg,[1] Erik van Meijgaard,[6] Isabella Velicogna,[3,4] Bert Wouters[5,6]

Mass budget calculations, validated with satellite gravity observations [from the Gravity Recovery and Climate Experiment (GRACE) satellites], enable us to quantify the individual components of recent Greenland mass loss. The total 2000–2008 mass loss of ~1500 gigatons, equivalent to 0.46 millimeters per year of global sea level rise, is equally split between surface processes (runoff and precipitation) and ice dynamics. Without the moderating effects of increased snowfall and refreezing, post-1996 Greenland ice sheet mass losses would have been 100% higher. Since 2006, high summer melt rates have increased Greenland ice sheet mass loss to 273 gigatons per year (0.75 millimeters per year of equivalent sea level rise). The seasonal cycle in surface mass balance fully accounts for detrended GRACE mass variations, confirming insignificant subannual variation in ice sheet discharge.

There are strong indications that mass loss from the Greenland ice sheet (GrIS) has recently accelerated (*1*–*3*) after atmospheric warming and increased runoff (*4*, *5*) and increased ice discharge through the acceleration of outlet glaciers in the west (*6*, *7*) and east (*8*–*11*). Recently reported GrIS mass balance (*12*) varies from near-balance (*13*) to modest mass losses [47 to 97 gigatons (Gt) year^{-1}] (*14*) in the 1990s, increasing to a mass loss of 267 ± 38 Gt year^{-1} in 2007 (*15*). These mass losses are equivalent to a global sea level rise (SLR) of 0.13 to 0.74 mm year^{-1} or 4 to 23% of the SLR of 3.1 ± 0.7 mm year^{-1} reported for the period 1993–2005 (*16*).

Here we present consistent 2003–2008 GrIS mass loss rates produced by two fully independent methods: The mass budget method, which quantifies the individual components of ice sheet mass balance [surface mass balance (SMB) and ice discharge (D)], is validated with data from the Gravity Recovery and Climate Experiment (GRACE) satellites, which observe ice sheet mass anomalies by repeat satellite gravimetry. This combination of results enables us to resolve the individual components of recent GrIS mass loss in space and time.

For SMB, we used the monthly output of a 51-year climate simulation (1958–2008) with the Regional Atmospheric Climate Model (RACMO2/GR) at high horizontal resolution (~11 km) (fig. S1). The modeled SMB from RACMO2/GR agrees very well with in situ observations [N = 265, correlation coefficient (r) = 0.95], without need for post-calibration (*17*). For D, we used ice flux data from 38 glacier drainage basins (*15*), covering 90% of the ice sheet (fig. S2), corrected for SMB between flux gate and grounding line and updated to include 2008. To compare SMB-D with GRACE requires the calculation of cumulative SMB-D anomalies. The temporal evolution of the cumulative SMB-D anomaly was evaluated using monthly GRACE mass changes (*18*). The spatial distribution of GrIS mass changes was compared to a regionally distributed GRACE solution (*19*), updated to include 2008. For more details on data and methods, see the supporting online material.

Figure 1 compares the time series of the cumulative SMB-D anomaly with GRACE data (*18*) in the epoch during which both are available (2003–2008). The high correlation (r = 0.99) between the two fully independent time series and the similarity in trends support the consistency of the mass balance reconstruction. A linear regression on the SMB-D time series yields a 2003–2008 GrIS mass loss rate of –237 ± 20 Gt year^{-1}.

A potential source of error is that the GRACE signal includes the seasonal cycles of supraglacial/englacial water storage and ice discharge (*20*–*22*). Because only a single discharge data point per year is available, we assume slow-

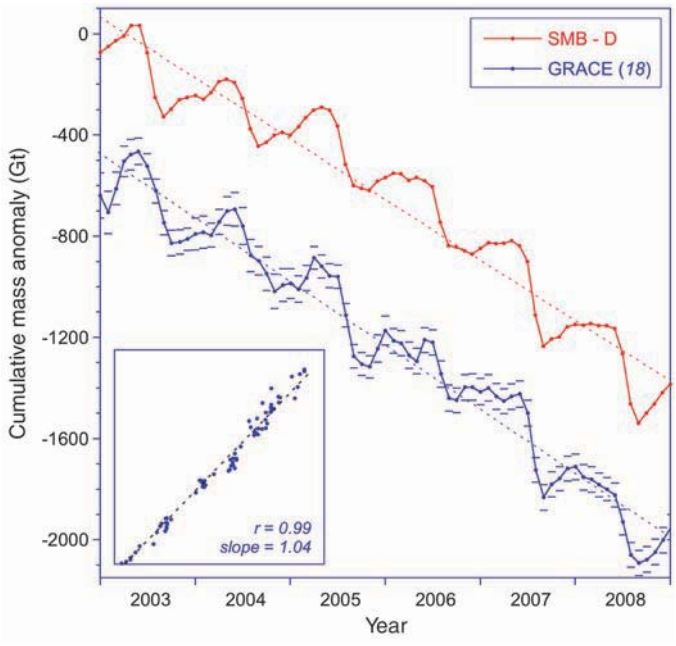

Fig. 1. Cumulative SMB-D anomaly (2003–2008) and comparison with GRACE data (*18*). Short horizontal lines indicate GRACE uncertainty, dashed lines the linear trends. GRACE values are not absolute numbers, and the curve has been vertically shifted for clarity. The scatter plot in the inset shows a direct linear regression between the monthly GRACE values as a function of the cumulative SMB-D anomaly, together with the linear regression coefficients.

[1]Institute for Marine and Atmospheric Research, Utrecht University, Netherlands. [2]Bristol Glaciology Centre, School of Geographical Sciences, University of Bristol, Bristol, UK. [3]Department of Earth System Science, University of California, Irvine, CA, USA. [4]Jet Propulsion Laboratory, Pasadena, CA, USA. [5]Delft Institute of Earth Observation and Space Systems, Delft University of Technology, Delft, Netherlands. [6]Royal Netherlands Meteorological Institute, De Bilt, Netherlands.

*To whom correspondence should be addressed. E-mail: m.r.vandenbroeke@uu.nl

ly changing ice flow without a seasonal cycle. The difference between the detrended GRACE and SMB time series, which represents these effects, shows no significant seasonal cycle. We confirm, therefore, that the influence of seasonal modulation of ice velocity on the ice sheet mass balance is insignificant (*2*, *7*).

A principal result is GrIS annual mass balance SMB-D (fig. S3 and eq. S1). Since 2000, GrIS mass balance has been persistently negative, caused by a simultaneous decrease in SMB and an increase in D. In total, the GrIS lost 1492 Gt between 2000 and 2008, or 166 Gt year^{-1}, equivalent to 0.46 mm year^{-1} of global SLR. Mass loss rate increased to 273 Gt year^{-1} in the period 2006–2008, equivalent to 0.75 mm year^{-1} of global SLR.

An important feature in fig. S3 is the large interannual variability of SMB, which may change by up to 400 Gt year^{-1} between consecutive years (standard deviation 107 Gt year^{-1}). Apart from the uncertainties involved in estimating mass balance components, this offers a partial explanation for the wide range of recently reported values of GrIS mass balance (*12*) and emphasizes the need for long-term observations.

The three main budgets that determine GrIS mass balance are ice sheet mass balance, SMB, and liquid water balance (eqs. S1 to S3). Our results show that both mass balance components, SMB and D (eq. S1), contributed equally to the post-1996 cumulative GrIS mass loss (Fig. 2A). Previous results (*15*) showed that discharge anomalies contributed 61% to recent GrIS mass loss; the shift to 50% can be fully explained by the larger interannual variability and the stronger downward trend in our updated SMB time series as compared to earlier estimates (*17*).

A quadratic decrease ($r^2 = 0.97$) explains the 2000–2008 cumulative mass anomaly better than a linear fit ($r^2 = 0.90$). Equation S1 implies that when SMB-D is negative but constant in time, ice sheet mass will decrease linearly in time. If, however, SMB-D decreases linearly in time, as has been approximately the case since 2000 (fig. S3), ice sheet mass is indeed expected to decrease quadratically in time.

The surface effects are further partitioned in Fig. 2B, detailing the contributions of the SMB components precipitation, sublimation, and runoff (eq. S2). Before 1996, decadal precipitation variability fully explained SMB anomalies. Between 1996 and 2004, large positive (~800 Gt) runoff and precipitation anomalies developed simultaneously. Because these approximately cancelled each other out, the SMB anomaly remained small during this period. After 2004, the cumulative precipitation anomaly no longer increased, but runoff remained high, resulting in an acceleration of GrIS mass loss, which was also detected by GRACE (*3*).

To further partition the runoff anomaly, Fig. 2C shows the main components of the liquid water balance: rain, melt, refreezing, and retention (eq. S3). After regional atmospheric warming (*4*, *5*), a cumulative meltwater anomaly of ~1900 Gt developed between 1996 and 2008, to which increased rainfall added another ~200 Gt. Only ~70% (1500 Gt) of this excess liquid water left the ice sheet as runoff, the remainder (~600 Gt) being refrozen in the firn layer. Since 1996, this refreezing anomaly has released ~2.0×10^{20} J of energy into the GrIS firn layer. Assuming the firn layer to be 100 m thick, to have an average density of 600 kg m^{-3}, and to cover 90% of the ice sheet surface, this is sufficient to heat up the entire firn column by 1 K. However, the refreezing anomaly

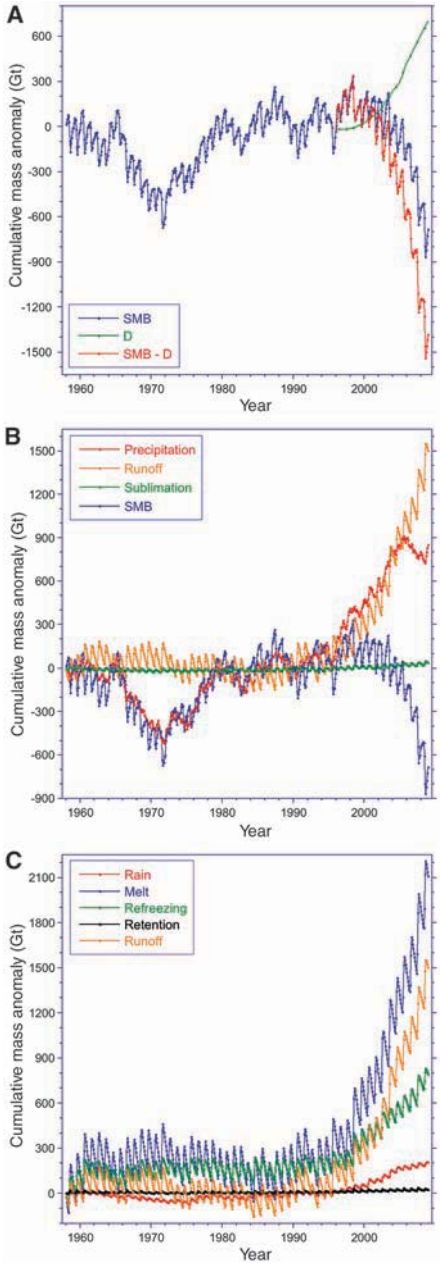

Fig. 2. Cumulative anomalies of the three main ice sheet mass budgets. (**A**) Mass balance and its components SMB and D (eq. S1). Before 1996, D and hence SMB-D, are poorly constrained and therefore not shown. (**B**) SMB and its components precipitation, runoff, and sublimation (eq. S2). (**C**) Liquid water balance and its main components rain, melt, refreezing, retention, and runoff (eq. S3).

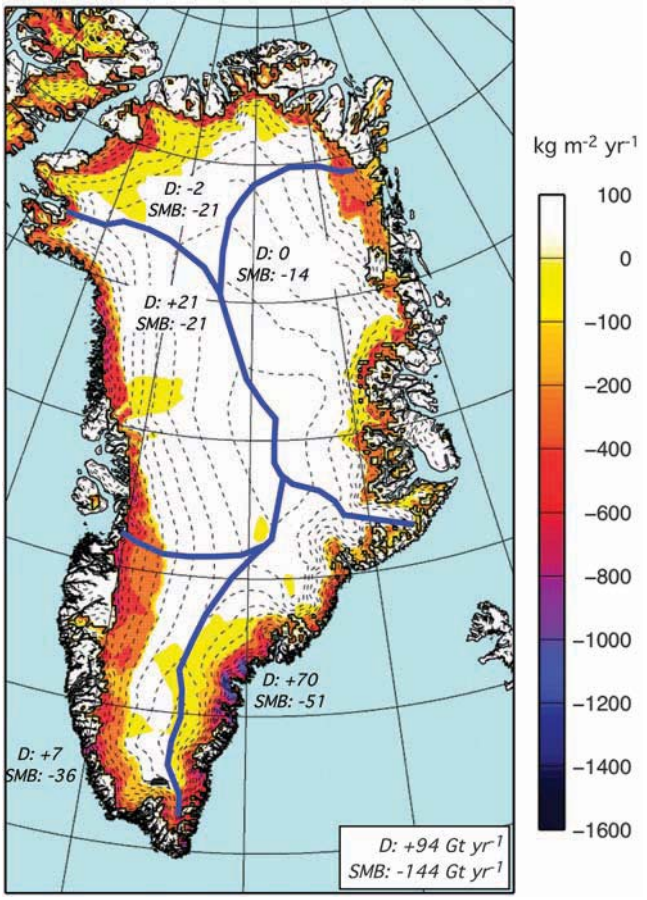

Fig. 3. Distribution of 2003–2008 mass changes across the ice sheet. The period (2003–2008) was chosen to coincide with the GRACE and IceSAT epochs. Numbers indicate basin-integrated mass loss rates due to SMB and D (in Gt year^{-1}). Numbers in the lower right corner represent the values for the whole ice sheet, indicating the dominant surface contribution to GrIS mass loss during 2003–2008. Colors represent the rate of surface mass change.

is not equally distributed over the GrIS, but concentrated in the lower accumulation zone. Our model data suggest that over the period 1990–2008, the first 15 m of the firn column in these areas has locally warmed by 5° to >10°. From Fig. 2, B and C, we conclude that, without the moderating effects of increased precipitation and refreezing, the post-1996 cumulative mass anomaly and associated SLR from the GrIS would have been 100% greater than actually observed.

The results also shed light on the relative timing of changes in surface conditions and ice dynamics. In central Greenland, enhanced surface melting started around 1996, several years before marine-terminating glaciers started to accelerate and retreat in the west (~1998) (*6*, *7*) and east (~2002) (*2*, *8*, *10*). In south Greenland, enhanced melting started in the early 1990s, but dynamic thinning was already active south of Helheim glacier in southeast Greenland (*23*, *24*).

To mimic the spatial distribution of GrIS mass loss during the GRACE and ICESat (Ice, Cloud, and Land Elevation Satellite) operational period, we performed a linear regression on 2003–2008 cumulative anomalies of D and SMB components, integrated over five major drainage basins (north, northeast, southeast, southwest, and northwest; fig. S2). The contributions from D and SMB to the basin-integrated mass change are given as numbers in Fig. 3, whereas the contributions from individual SMB components are listed in table S1.

In the north and northeast, which are regions with low accumulation and hence low rates of ice discharge, the discharge anomaly is small, and above-normal runoff dominated 2003–2008 mass loss. In the southwest, the ablation area is relatively large, with few marine-terminating glaciers; here, meltwater production and ice flow strongly interact (*20*–*22*), and increased discharge also contributed to the mass loss. In the northwest, which harbors numerous tidewater glaciers, mass loss is equally distributed between surface processes and ice discharge. In these four basins, surface mass losses represent increased runoff, moderated by above-normal snowfall (table S1).

The greatest 2003–2008 basin mass loss, representing about half of the ice sheet total, is found in the very wet southeast. Here, ice discharge dominates the signal. This is the only basin where the trend in the cumulative precipitation anomaly is negative, after anomalously high snowfall in this region from September 2002 to April 2003 (*25*), just at the onset of the GRACE period. As a result, the surface mass loss in the southeast is equally split between above-normal runoff and below-normal precipitation (table S1). Without the precipitation anomaly, the 2003–2008 mass loss rate in the southeast would have been ~20% smaller.

The colors in Fig. 3 represent surface mass loss rate (2003–2008). Because surface mass loss is dominated by runoff, it is heavily concentrated in the ablation zone of the ice sheet, roughly below 2000 m above sea level (asl). Surface mass loss rates range from 200 to 600 kg m^{-2} $year^{-1}$ in the northern and western ablation zones, and locally exceed 600 kg m^{-2} $year^{-1}$ in the southeast, owing to the effect of decreased precipitation. Assuming (conservatively) the surface mass loss to occur at the density of ice (910 kg m^{-3}), they account for >60 cm $year^{-1}$ of surface lowering locally in the southeast and 20 to 60 cm $year^{-1}$ elsewhere in the GrIS ablation zone. This explains part of the 2003–2008 thinning pattern as observed by the IceSAT and ASTER (Advanced Spaceborne Thermal Emission and Reflection Radiometer) satellites (*26*, *27*), noting that the strong thinning of the fastest-flowing parts of many outlet glaciers, up to several meters per year, remains dominated by dynamic processes. Figure 3 resembles the spatial GrIS mass loss pattern observed by GRACE (*19*), with mass losses concentrated in the southeast, northwest, and southwest at elevations below 2000 m asl.

The good agreement between mass budget calculations and the GRACE data enables us to make a detailed interpretation of the GRACE signal in terms of its individual components. Examining the period with well-constrained discharge data (1996–2008, fig. S4), we see that the ice sheet–integrated GRACE signal primarily consists of (i) the slowly changing ice discharge anomaly, (ii) the asymmetric yet regular sawtooth shape of the seasonal runoff anomaly, and (iii) noise from precipitation variability on monthly to decadal time scales.

References and Notes

1. R. Thomas, E. Frederick, W. Krabill, S. Manizade, C. Martin, *Geophys. Res. Lett.* **33**, L10503 (2006).
2. E. Rignot, P. Kanagaratnam, *Science* **311**, 986 (2006).
3. I. Velicogna, J. Wahr, *Nature* **443**, 329 (2006).
4. J. E. Box, A. E. Cohen, *Geophys. Res. Lett.* **33**, L12706 (2006).
5. E. Hanna *et al*., *J. Clim.* **21**, 331 (2008).
6. I. Joughin, W. Abdalati, M. Fahnestock, *Nature* **432**, 608 (2004).
7. A. Luckman, T. Murray, *Geophys. Res. Lett.* **32**, L08501 (2005).
8. A. Luckman, T. Murray, R. de Lange, E. Hanna, *Geophys. Res. Lett.* **33**, L03503 (2006).
9. L. A. Stearns, G. S. Hamilton, *Geophys. Res. Lett.* **34**, L05503 (2007).
10. I. M. Howat, I. Joughin, S. Tulaczyk, S. Gogineni, *Geophys. Res. Lett.* **32**, L22502 (2005).
11. I. M. Howat, I. Joughin, T. Scambos, *Science* **315**, 1559 (2007).
12. A. Cazenave, *Science* **314**, 1250 (2006).
13. H. J. Zwally *et al*., *J. Glaciol.* **51**, 509 (2005).
14. W. Krabill *et al*., *Science* **289**, 428 (2000).
15. E. Rignot, J. E. Box, E. Burgess, E. Hanna, *Geophys. Res. Lett.* **35**, L20502 (2008).
16. N. L. Bindoff *et al*., in *Climate Change 2007: The Physical Science Basis* (Cambridge Univ. Press, Cambridge, 2007), pp. 385–432.
17. J. Ettema *et al*., *Geophys. Res. Lett.* **36**, L12501 (2009).
18. I. Velicogna, *Geophys. Res. Lett.* **36**, L19503.
19. B. Wouters, D. Chambers, E. J. O. Schrama, *Geophys. Res. Lett.* **35**, L20501 (2008).
20. H. J. Zwally *et al*., *Science* **297**, 218 (2002).
21. R. S. W. van de Wal *et al*., *Science* **321**, 111 (2008).
22. I. Joughin *et al*., *Science* **320**, 781 (2008).
23. W. Krabill *et al*., *Science* **283**, 1522 (1999).
24. E. Rignot, D. Braaten, S. P. Gogineni, W. B. Krabill, J. R. McConnell, *Geophys. Res. Lett.* **31**, L10401 (2004).
25. J. E. Box *et al*., paper presented at the 8th International Conference on Polar Meteorology and Oceanography, San Diego, CA, 9 to 13 January 2005.
26. D. C. Slobbe, R. C. Lindenbergh, P. Ditmar, *Remote Sens. Environ.* **112**, 4204 (2008).
27. I. M. Howat, B. E. Smith, I. Joughin, T. A. Scambos, *Geophys. Res. Lett.* **35**, L17505 (2008).

28. This work is funded by Utrecht University (M.v.d.B. and W.J.v.d.B.) and the Netherlands Polar Program of the Netherlands Organization of Scientific Research (NWO/ALW) through the international RAPID project (J.E.), UK Natural Environment Research Council grant NE/C509474/1 (J.L.B.), the Royal Netherlands Meteorological Institute (E.v.M.), and Netherlands Institute for Space Research grant SRON/EO-076 (B.W.). E.R. and I.V. performed their work at the University of California, Irvine, and Caltech's Jet Propulsion Laboratory under a contract with NASA's Cryosphere Science Program. Climate data are available from the RAPID data repository at the British Atmospheric Data Centre (badc.nerc.ac.uk).

Supporting Online Material

www.sciencemag.org/cgi/content/full/326/5955/984/DC1
Data and Methods
Figs. S1 to S4
Table S1
References

24 June 2009; accepted 8 September 2009
10.1126/science.1178176

$CD4^+$ Regulatory T Cells Control T_H17 Responses in a Stat3-Dependent Manner

Ashutosh Chaudhry,[1,2] Dipayan Rudra,[1,2] Piper Treuting,[3] Robert M. Samstein,[1] Yuqiong Liang,[1] Arnold Kas,[2] Alexander Y. Rudensky[1,2]*

Distinct classes of protective immunity are guided by activation of STAT transcription factor family members in response to environmental cues. $CD4^+$ regulatory T cells (T_{regs}) suppress excessive immune responses, and their deficiency results in a lethal, multi-organ autoimmune syndrome characterized by T helper 1 (T_H1) and T helper 2 (T_H2) $CD4^+$ T cell–dominated lesions. Here we show that pathogenic T_H17 responses in mice are also restrained by T_{regs}. This suppression was lost upon T_{reg}-specific ablation of Stat3, a transcription factor critical for T_H17 differentiation, and resulted in the development of a fatal intestinal inflammation. These findings suggest that T_{regs} adapt to their environment by engaging distinct effector response–specific suppression modalities upon activation of STAT proteins that direct the corresponding class of the immune response.

The vertebrate immune system affords defense against different classes of pathogens by activation of a particular type of immune response. Intracellular pathogens induce protective T_H1 responses, whereas parasitic helminthes induce T_H2 cytokine production. In contrast, pathogenic yeast, fungi, and extracellular bacteria elicit highly inflammatory T_H17